THE JOURNAL OF PHYSICAL CHEMISTRY A

ARTICLE

pubs.acs.org/JPCA

On the Excited State Dynamics of Vibronic Transitions. High-Resolution Electronic Spectra of Acenaphthene and Its Argon van der Waals Complex in the Gas Phase

Leonardo Álvarez-Valtierra*

División de Ciencias e Ingenierías, Campus León, Universidad de Guanajuato, León, Gto. 37150, México

David F. Plusquellic

Optical Technology Division, Physical Measurement Laboratory, National Institute of Standards and Technology, Gaithersburg, Maryland 20899, United States

John T. Yi

Department of Chemistry, Winston-Salem State University, Winston-Salem, North Carolina 27110, United States

David W. Pratt

Department of Chemistry, University of Pittsburgh, Pittsburgh, Pennsylvania 15260, United States

ABSTRACT: Rotationally resolved fluorescence excitation spectroscopy has been used to study the dynamics, electronic distribution, and the relative orientation of the transition moment vector in several vibronic transitions of acenaphthene (ACN) and in its Ar van der Waals (vdW) complex. The 0_0^0 band of the $S_1 \leftarrow S_0$ transition of ACN exhibits a transition moment orientation parallel to its *a*-inertial axis. However, some of the vibronic bands exhibit a transition moment orientation parallel to the *b*-inertial axis, suggesting a Herzberg−Teller coupling with the S_2 state. Additionally, some other vibronic bands exhibit anomalous intensity patterns in several of their rotational transitions. A Fermi resonance involving two near degenerate vibrations has been proposed to explain this behavior. The high-resolution electronic spectrum of the ACN−Ar vdW complex has also been obtained and fully analyzed. The results indicate that the weakly attached argon atom is located on top of the plane of the bare molecule at ∼3.48 Å away from its center of mass in the S_0 electronic state.

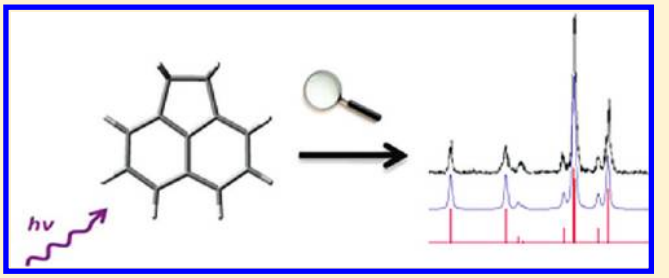

1. INTRODUCTION

Naphthalene (NAPH) has been extensively investigated over the past five decades using a variety of spectroscopic techniques to determine the symmetry properties of its lowest electronically excited states. The lowest $\pi\pi^*$ transition of NAPH at 32020.2 cm^{-1} is weak and has a transition dipole moment orientation (TDM) along the long in-plane (*a*-inertial axis), identifying the electronic state as a $^1B_{3u}$ (^1L_b), whereas the next $\pi\pi^*$ transition in NAPH at 35900 cm^{-1} is strong, *b*-axis polarized, and identified as a $^1B_{2u}$ (^1L_a) excited electronic state.[1−3] These findings have been confirmed by high-resolution electronic spectroscopy experiments in the gas phase.[4] Several additional high resolution studies have reported that the electronic state properties of 1-substituted naphthalenes are similar to those of the parent molecule[5−7] whereas those of 2-substituted naphthalenes are quite different. For the latter, the TDMs of the $S_1 \leftarrow S_0$ origin transitions exhibit *b*-axis orientations because of the different nodal properties of their frontier molecular orbitals (MOs).[8] 1-Aminonaphthalene is an exception to this rule; its $S_1 \leftarrow S_0$ transition is mostly *b*-axis polarized,[9] suggesting a reversal of the ^1L_b and ^1L_a states owing to the conjugative properties of the amino group.

Azulene,[10] anthracene,[11] phenanthrene,[12] tetracene,[13] pyrene,[14] and perylene[15] are other polycyclic aromatic hydrocarbons (PAHs) that have been studied by high-resolution electronic spectroscopy in the gas phase. In this report, we focus on another such molecule, acenaphthene (ACN), shown below. While not strictly aromatic (the two bridging carbon atoms form sp^3 hybridized $-CH_2-$ groups), ACN possesses many of the same

Special Issue: David W. Pratt Festschrift

Received: December 31, 2010
Revised: May 6, 2011
Published: June 13, 2011

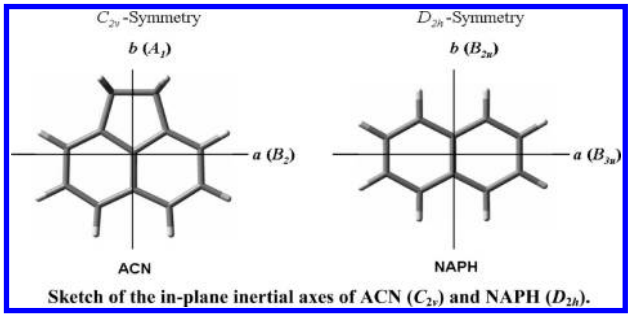

symmetry elements as naphthalene and, as will be seen, absorbs light in the same region of the electromagnetic spectrum. But ACN is a C_{2v} molecule, not D_{2h}, and thus we expect the lowest $\pi\pi^*$ transition of ACN to be perturbed with respect to that of NAPH and perhaps to exhibit a number of dynamical properties that are very different from those of the parent molecule. In this respect, it may resemble another molecule previously studied by this group, 9,10-dihydrophenanthrene (DHPH).[16]

2. EXPERIMENTAL SECTION

ACN (99% pure) was purchased from Aldrich and used without further purification. In the vibrationally resolved experiments, the sample was seeded into ~1200 Torr of argon gas and expanded into a vacuum chamber (10^{-5} Torr) through a 1 mm diameter orifice pulsed valve (General Valve Series 9) operating at 10 Hz. Two centimeters downstream of the valve, the sample was excited with the second harmonic of a Quanta Ray Nd^{3+}:YAG (Model DCR-1A) pumped dye laser (Model PDL-1). The dye (DCM) laser output was frequency doubled with an external KDP crystal providing a spectral resolution of ~0.6 cm^{-1} in the ultraviolet. From the point of intersection between the nozzle and the laser, the molecules were excited and the fluorescence was collected with a photomultiplier tube (PMT). Finally, the collected data were processed by a boxcar integrator (Stanford Research Systems) and recorded with Quick Data Acquisition software version 1.0.5.

Rotationally resolved experiments were performed using a molecular beam laser spectrometer, described in detail elsewhere.[17] Briefly, the molecular beam was formed by coexpansion of the vaporized sample and an argon carrier gas (~300 Torr) through a heated (~313 K) 240 μm quartz nozzle into a differentially pumped vacuum system. Two different kinds of experiments were performed. The bare ACN molecule was studied in the high-resolution port; here, the expansion was skimmed twice and crossed 110 cm downstream by a continuous wave (CW) Ar^+ pumped ring dye laser. The ACN−Ar complex was studied in the low-resolution port; here, the expanding gas was skimmed only once and crossed 15 cm downstream by the laser beam. The CW laser was operated with DCM special dye and was intracavity frequency doubled in either a 630 nm $LiIO_3$ or a 620 nm BBO crystal, yielding approximately 350 μW of UV radiation with a resolution of ~1 MHz. The fluorescence excitation spectrum was detected by a PMT and photon counting system using spatially selective optics. This signal, together with the iodine absorption spectrum and the relative frequency markers, was simultaneously collected and processed by the JBA95 data acquisition system.[17] Absolute frequency calibration of the spectra was performed by comparison with the I_2 absorption spectrum.[18] Relative frequency markers were obtained from a stabilized etalon having a free spectral range of 299.7520 ± 0.0005 MHz in the fundamental of the dye.

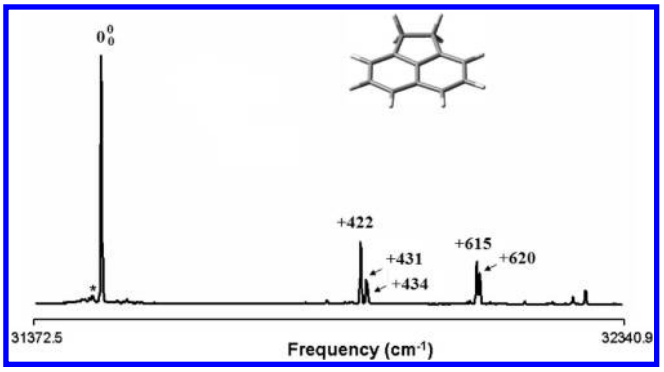

Figure 1. Vibrationally resolved fluorescence excitation spectrum of acenaphthene (ACN) in a supersonic jet. The small transition marked with the asterisk is the origin band of the argon complex.

3. RESULTS

Figure 1 shows the vibrationally resolved fluorescence excitation spectrum of jet-cooled ACN in the gas phase. In agreement with previous results,[19,20] we observe that the electronic origin (0_0^0 band) of ACN is red shifted by ~542 cm^{-1} from that of NAPH, but is much stronger in relative intensity.[3,4] Frequency labels are used to identify the stronger vibronic bands in the spectrum. The group of bands located at 422−434 cm^{-1} in Figure 1 is close in frequency to the 8_0^1 vibronic band, the strongest band in the spectrum of NAPH, one of which should be the corresponding analog. Interestingly, the remaining vibronic bands in the spectrum of Figure 1 were not detected in the low-resolution spectrum of the parent molecule, NAPH.[2,3]

Rotationally resolved studies have been performed on every single labeled band in Figure 1, to investigate the origin of such transitions and provide further information about other phenomena that might occur upon excitation with light. Figure 2 shows the rotationally resolved $S_1 \leftarrow S_0$ fluorescence excitation spectrum of the 0_0^0 band of ACN at 31477.1 cm^{-1}. The spectrum spans approximately 3.5 cm^{-1} and exhibits pure *a*-type character; that is, the TDM vector lies parallel to the *a*-inertial axis of the molecule. To fit this spectrum, we first generated ~3000 *a*-type rovibronic transitions based on ab initio[21] estimates of rotational constants and rigid rotor Hamiltonians for both electronic states. Then, we made quantum number assignments of single transitions in the simulated spectrum to the corresponding transitions in the experimental spectrum, using the Windows-based program JB95.[22] Finally, we used a least-squares fitting procedure to optimize the rotational constants, based on comparisons of the observed and calculated line positions. The final fit utilized 300 assigned lines and resulted in a standard deviation (OMC) of 1.9 MHz. The quality of the fit is shown in the bottom panel of Figure 2. Here, trace 1 shows a portion of the Q branch of the fully resolved experimental spectrum, and traces 2 and 3 show the simulated spectra. Trace 3 is in a "stick-type" spectrum and trace 2 is the simulation with a Voigt line shape function applied (3 MHz Gaussian and 2 MHz Lorentzian contributions) with a FWHM line width of 2.7 MHz. The rotational temperature of the fit is 3.5 K. The inertial parameters of this band are summarized in Table 1.

Figures 3 and 4 show the high-resolution spectra of three vibronic bands of ACN at +422, 431, and 434 cm^{-1} above the origin band. Surprisingly, all three of these bands exhibit *b*-axis polarized spectra. Therefore, their TDMs are parallel to the C_2

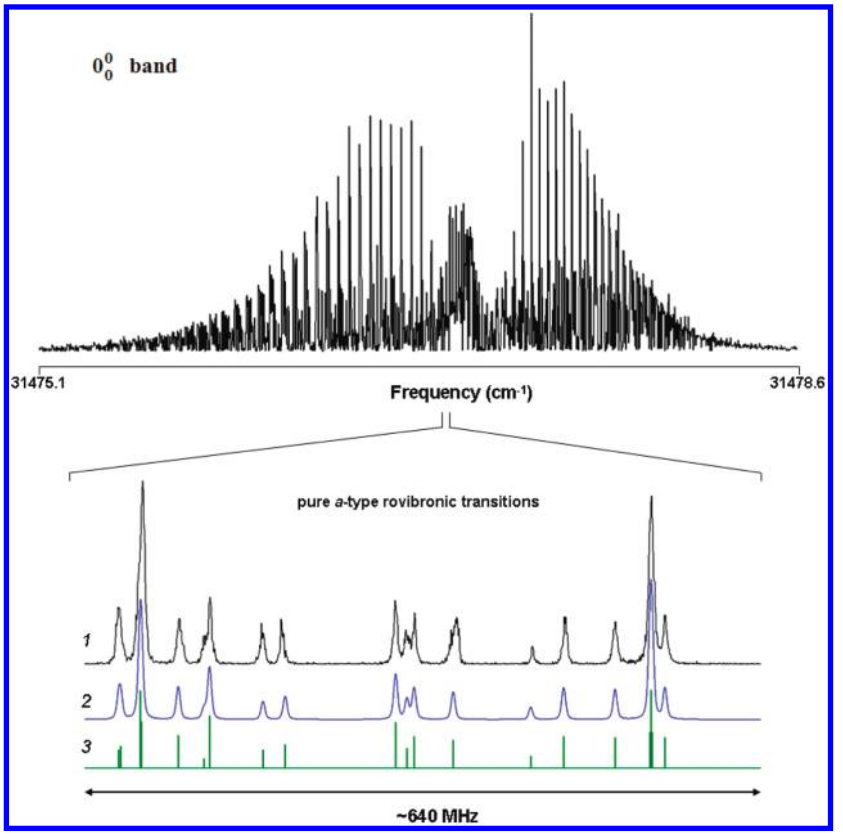

Figure 2. Rotationally resolved fluorescence excitation spectrum of the $S_1 \leftarrow S_0$ electronic origin band of ACN. A portion of the fully resolved experimental spectrum (1) and the corresponding simulated spectrum with (2) and without (3) a convoluted line shape function, are also shown in the bottom panel.

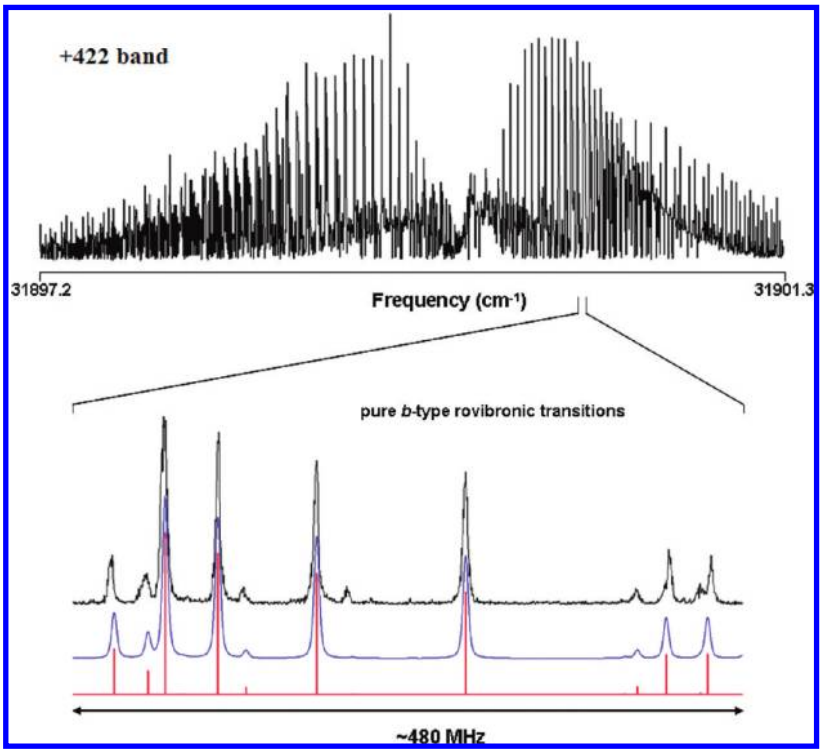

Figure 3. Rotationally resolved fluorescence excitation spectrum of the +422 band of ACN. A portion of the fully resolved experimental spectrum and the corresponding simulated spectrum are also shown in the bottom panel.

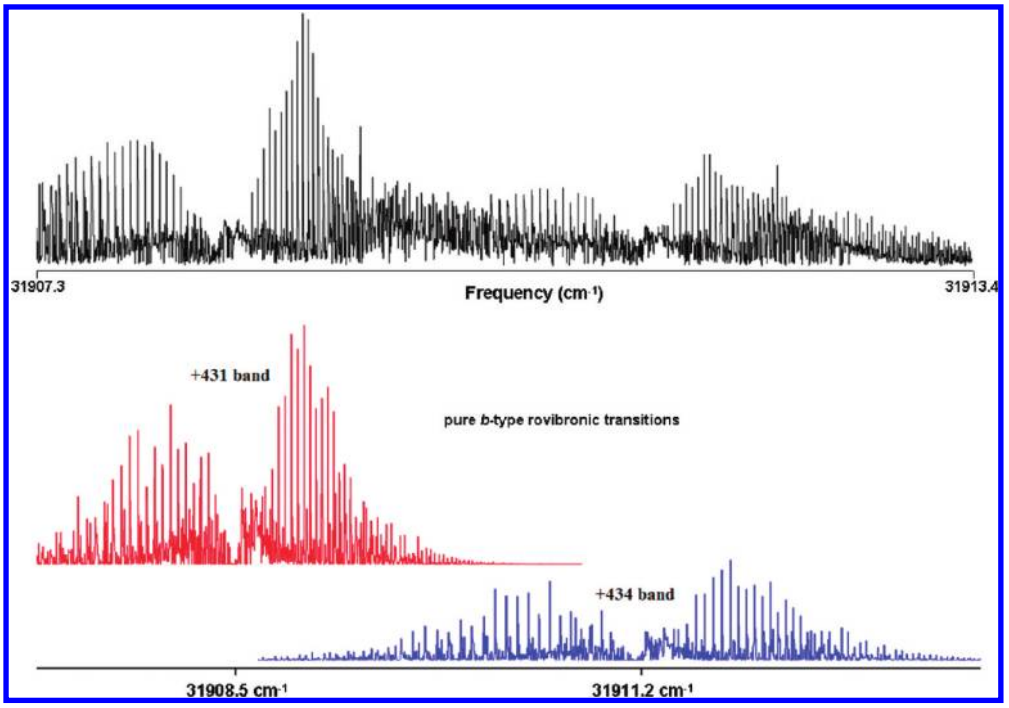

Figure 4. Rotationally resolved fluorescence excitation spectra of the +431 and 434 bands of ACN. The two simulated spectra are shown in the bottom panel.

symmetry axis of the molecule, not perpendicular to it, as in the case of the origin band. Analyses of these spectra proceeded in a manner similar to the previously described origin band. In the case of the +422 band (see Figure 3), ~6800 *b*-type rovibronic transitions were simulated. Of these, 200 lines were assigned and fit using rigid rotor Hamiltonians for both electronic states. In the bottom panel of Figure 3, the experimental trace and the corresponding simulations, with and without a line shape function, are also shown. The OMC of the fit is 1.49 MHz, the Voigt profile of the line shape has 3 MHz Gaussian and 2 MHz Lorentzian contributions. The rotational temperature of the fit is 8 K. For the +431 and +434 bands (see Figure 4), 220 lines out of ~7500 were assigned, resulting in standard deviations of 1.5 MHz; the rotational temperatures of the fits are 9.5 and 17 K, respectively. Voigt profile components similar to those used in the +422 band were used in these fits. The bottom panel of Figure 4 shows two simulated spectra for each experimental transition along with their corresponding frequency origin. The inertial parameters of these three bands are also reported in Table 1.

Two higher vibronic transitions (+615 and 620 bands in Figure 1) of ACN also were fully analyzed at rotational resolution. Both of these transitions exhibit parallel polarizations.

Table 1. Inertial Parameters of the Origin Band and Some Higher S_1 Vibronic Bands of Acenaphthene

parameter[a,b]	0_0^0	+422.4	+431.4	+434.2	+615.5	+620.3
S_0						
A'' (MHz)	1410.3 (1)	1410.3 (1)	1410.3 (1)	1410.7 (1)	1410.2 (1)	1410.2 (1)
B'' (MHz)	1193.9 (1)	1193.9 (1)	1193.9 (1)	1194.2 (1)	1193.8 (1)	1193.8 (1)
C'' (MHz)	652.0 (1)	652.0 (1)	652.0 (1)	652.3 (1)	652.1 (1)	652.0 (1)
$\Delta I''$ (u Å^2)	−6.58 (2)	−6.58 (2)	−6.59 (2)	−6.61 (2)	−6.63 (2)	−6.62 (2)
S_1						
A' (MHz)	1394.1 (1)	1394.6 (1)	1394.3 (1)	1394.8 (1)	1393.4 (1)	1393.3 (1)
B' (MHz)	1175.8 (1)	1176.0 (1)	1176.0 (1)	1176.4 (1)	1176.2 (1)	1176.2 (1)
C' (MHz)	643.2 (1)	643.1 (1)	643.7(1)	644.0 (1)	643.4 (1)	643.3 (1)
$\Delta I'$ (u Å^2)	−6.56 (2)	−6.25 (2)	−7.04 (2)	−7.18 (2)	−6.87 (2)	−6.84 (2)
band type	*a*	*b*	*b*	*b*	*a*	*a*
band origin (cm^{-1})	31477.11	31899.53	31908.52	31911.26	32092.56	32097.38
OMC (MHz)	1.94	1.49	1.52	1.40	1.40	1.25
temp (K)	3.5	8.0	9.5	17.0	11.0	11.0

[a] Standard deviations shown in parentheses are relative to the last significant figure. [b] MP2/6-31G** values: A'' = 1410.1, B'' = 1194.4, and C'' = 651.8 MHz.

dx.doi.org/10.1021/jp1124298 |*J. Phys. Chem. A* 2011, 115, 9557–9566

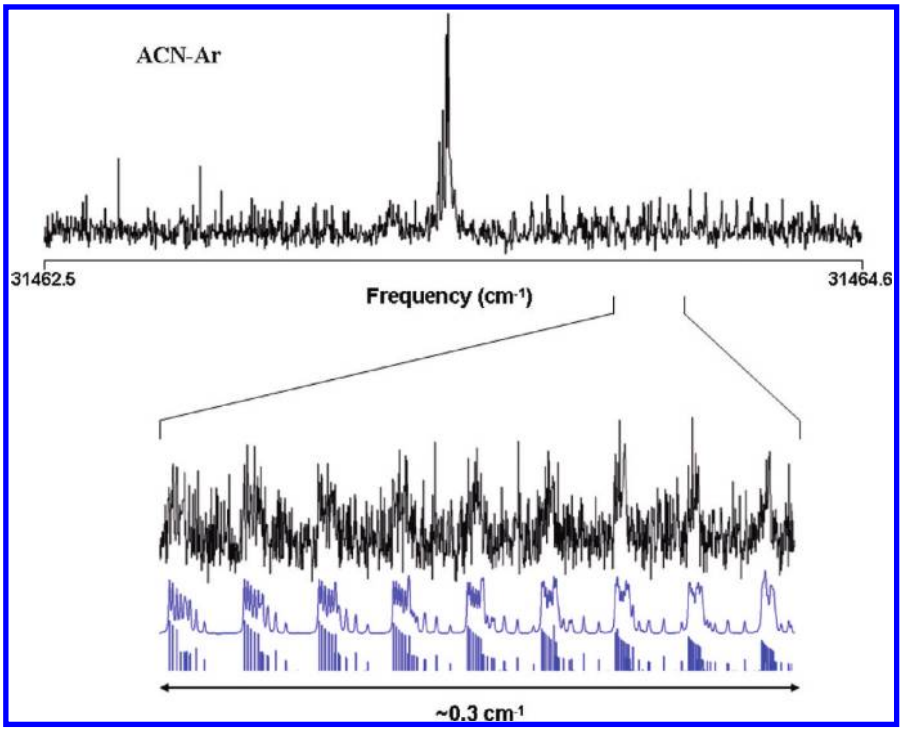

Figure 5. Rotationally resolved fluorescence excitation spectrum of the ACN−Ar vdW complex in the gas phase. A portion of the fully resolved experimental spectrum and the corresponding simulation are also shown in bottom panel.

Therefore, their band contours are similar to that shown in Figure 2 for the 0_0^0 band. However, the two vibronic bands exhibit significant perturbations in their rotational structure. Their experimental spectra exhibit rotational line intensities that cannot be simulated using rigid rotor Hamiltonians at any rotational temperature. Moreover, attempts to fit a few of the transitions exhibiting anomalous frequency shifts (especially lines where $K_c' = 10$) with a Watson distortion Hamiltonian[23] for the S_1 state also were unsuccessful. Nonetheless, ignoring the very few shifted transitions, fits have been performed for these bands by assigning 800 lines of the ∼8500 simulated rovibronic transitions. The standard deviations of these fits are 1.40 and 1.25 MHz for the +615 and 620 bands, respectively. The Voigt line shape profiles required 3 MHz Gaussian and 4 MHz Lorentzian contributions. The rotational temperature that best fit the observed line intensities in both spectra was 11(2) K. The inertial parameters of these bands are included in Table 1.

Figure 5 shows the rotationally resolved fluorescence excitation spectrum of the weak band that is red shifted by 13.6 cm^{-1} from the 0_0^0 band of the bare molecule, marked by an asterisk in Figure 1. This spectrum spans about 2 cm^{-1} and exhibits *a*/*c*-type hybrid character. Again, this spectrum could not be fit using rigid rotor Hamiltonians, but in this case the Watson Hamiltonian[23] satisfactorily accounted for all observed lines. The standard deviation of the fit is 4.0 MHz and the Voigt profile for the line shape function required 22 MHz Gaussian and 3 MHz Lorentzian components. The rotational temperature of the fit is 5 K. From the spectral analysis, the obtained rotational constants are very close to the ab initio calculations for the ACN−Ar van der Waals (vdW) complex; see Table 2. The change in band polarization is consistent with this view. Therefore, the transition has been assigned as the $S_1 \leftarrow S_0$ origin band of the ACN−Ar vdW complex.

Table 2. Inertial Parameters of the Acenaphthene−Argon vdW Complex

parameter[a]	ACN-Ar[b] (experiment)	MP2/6-31G** (theory)
S_0		
A'' (MHz)	681.6 (1)	678.1
B'' (MHz)	666.2 (1)	644.4
C'' (MHz)	616.1 (1)	588.8
$\Delta I''$ (u Å^2)	−679.78 (2)	−671.31
S_1		
A' (MHz)	682.1 (1)	
B' (MHz)	658.1 (1)	
C' (MHz)	614.9 (1)	
$\Delta I'$ (u Å^2)	−687.02 (2)	
band type *a*/*b*/*c*	90/0/10	
band origin (cm^{-1})	31463.52	
OMC (MHz)	3.98	
temp (K)	5.0	

[a] Standard deviations shown in parentheses are relative to the last significant figure. [b] The following Watson distortion terms were required in the fit: $\Delta J'' = 0.00236$, $\Delta JK'' = -0.00671$, $\Delta K'' = 0.00193$, $\delta J'' = -0.00065$, $\delta K'' = -0.00351$ MHz; $\Delta J' = 0.00235$, $\Delta JK' = -0.00256$, $\Delta K' = -0.01039$, $\delta J' = -0.00094$, and $\delta K' = -0.00087$ MHz.

4. DISCUSSION

Nature of the S_1 State. The 0_0^0 band of ACN was experimentally found to be polarized parallel to the *a*-inertial axis of the molecule; that is, no *b*- or *c*-type rovibronic transitions were observed in the high resolution spectrum of Figure 2. This finding indicates that the S_1 electronic state of ACN is an ^1L_b

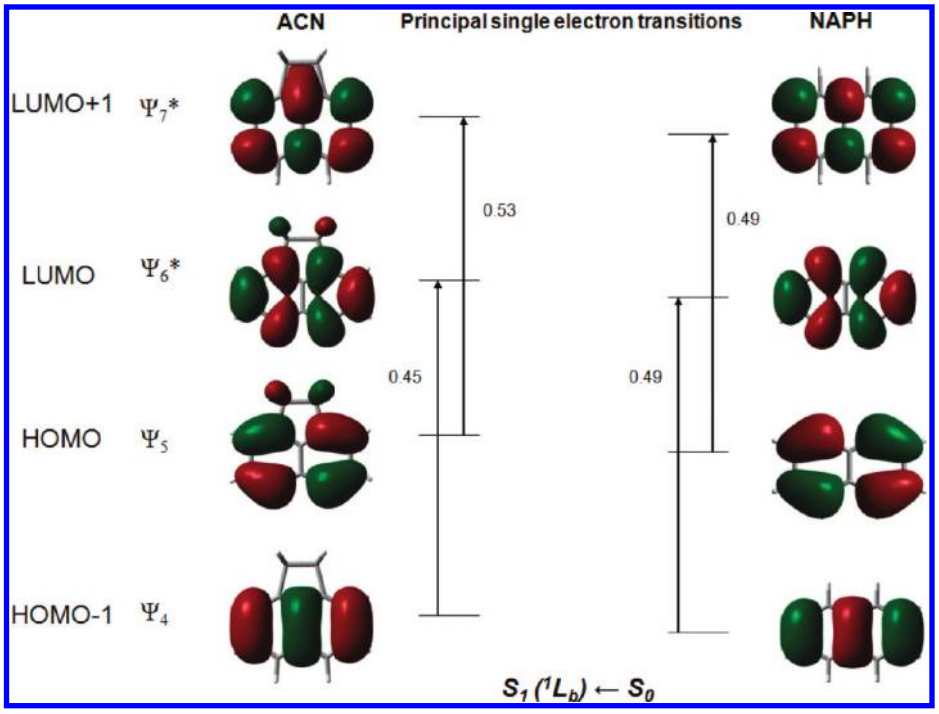

Figure 6. CIS/6-31G** frontier molecular orbitals of acenaphthene (ACN) and naphthalene (NAPH). The energy level diagrams indicate the principal single electronic transitions and their corresponding contributions to the $S_1 \leftarrow S_0$ electronic excitation.

(B_2) state, analogous to the *a*-type polarized 0_0^0 band found in NAPH.[1,2,24] However, the intensity of the origin band of ACN, compared to the intensity of the remaining vibronic bands in the spectrum, is considerably higher than the corresponding band in NAPH. This intensity enhancement is believed to be a consequence of the lower symmetry of the ACN molecule.

To explore this issue further, ab initio calculations[21] were performed to determine the properties of the MOs that participate in the $S_1 \leftarrow S_0$ transition. These are shown in Figure 6; the corresponding MOs of NAPH are shown for comparison. According to CIS, the principal one-electron excitations that contribute to the S_1 state are the LUMO+1 ← HOMO and LUMO ← HOMO−1 transitions. The oscillating charge distributions that are associated with these excitations are oriented along the *a*-inertial axis, as shown in Figure 7. Thus, the calculations agree with experiment; the excited S_1 state of ACN is predicted to be a ^1L_b state (B_2 symmetry in C_{2v} point group),[24] as in the case of NAPH. However, the calculations also predict that the two one-electron excitations contribute unequally to the S_1 state of ACN; ∼ 53% LUMO+1 ← HOMO, and ∼45% LUMO ← HOMO−1. In NAPH, the contributions of these two excitations are more nearly equal, resulting in an "out-of-phase" cancellation and an essentially "forbidden" 0_0^0 band.[5]

Analyses of the inertial parameters of the 0_0^0 band (cf. Table 1) reveal that ACN is a near-oblate asymmetric top with $\kappa'' = 0.429$. The calculated rotational constants[21] of the molecule in its ground state are in excellent agreement with the experimental values. Generally, the excited state A', B', and C' values are smaller than their ground state counterparts, owing to small ring expansions that are typical of $\pi\pi^*$ states; $\Delta A = (A' - A'') = -16.21$ MHz, $\Delta B = -18.07$ MHz, and $\Delta C = -8.87$ MHz. The observed changes in rotational constants are consistent with the nodes observed in the frontier molecular orbitals in Figure 6; upon excitation, the number of nodes increase in directions

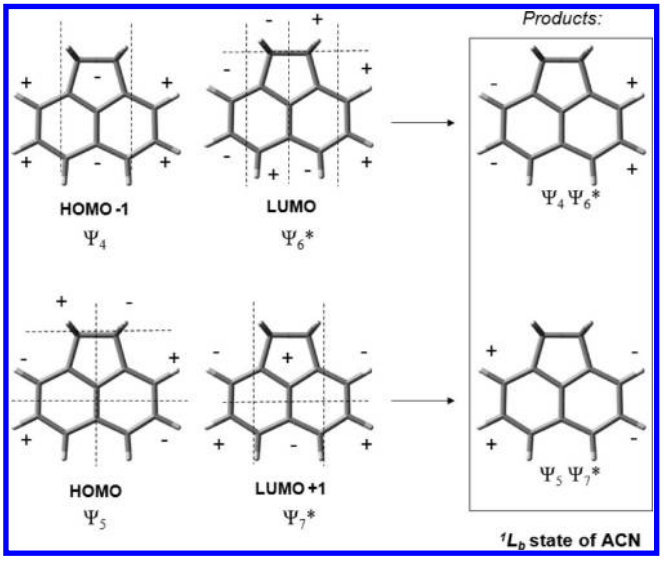

Figure 7. Product wave functions of acenaphthene in its $S_1 \leftarrow S_0$ electronic transition.

perpendicular to the *b*-axis of the molecule; the number of nodes also increase in directions perpendicular to the *a*-axis of the molecule, but to a lesser extent; and no evident changes are noticed in directions perpendicular to the *c*-axis.

Apparently, ACN is nonplanar in both electronic states. It has an inertial defect of −6.58 u Å^2 in its ground state, a value that is consistent with four hydrogen atoms out-of-plane of the concatenated planar ring moiety; this value does not change substantially when the molecule absorbs light.

Dynamics. The vibronic transitions of electronically excited states have been a topic of significant interest in the past few

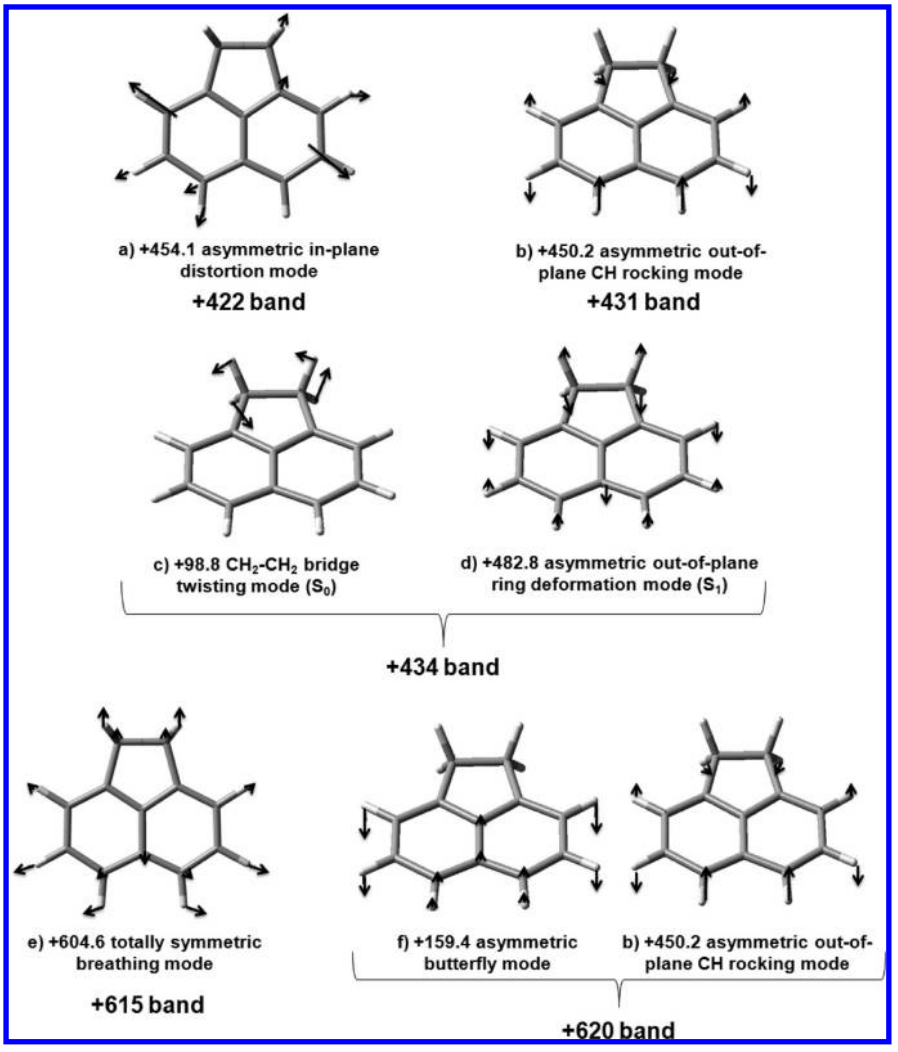

Figure 8. CIS/6-31G** vibrational modes of acenaphthene in its S_1 state and their experimental vibronic band assignments.

years. In one such study, significant state mixing was detected in the high resolution $S_1 \leftarrow S_0$ electronic spectra of fluorene, carbazole, and dibenzofuran.[25] Measurements of the TDM orientations of their origin bands show that the S_1 state of fluorene is a ^1L_b state whereas the S_1 states of carbazole and dibenzofuran are ^1L_a states, in Platt's notation.[26] However, measurements of the TDM orientations of several vibronic bands showed that one band in each spectrum exhibits a TDM orientation which is different from that of the origin band. These findings provide compelling evidence for an interaction between the vibronic transition and a second nearby electronic excited state (S_2, ^1L_a in fluorene and ^1L_b in carbazole and dibenzofuran) via Herzberg−Teller (HT) coupling.[27] More recently, the signatures of a conical intersection involving the ^1L_b and ^1L_a states of indole were discovered in the high resolution spectra of several vibronic bands in its $S_1 \leftarrow S_0$ transition,[28] but not in other indole derivatives with larger S_2/S_1 energy gaps.[29] The existence of such mixed states is a necessary prerequisite to photoinduced dynamical behaviors in the isolated molecules.

In ACN, the +422, 431, and 434 cm^{-1} vibronic bands were found to be polarized parallel to the *b*-inertial axis of the molecule (see Figures 3 and 4). The first two bands exhibit the same ground state rotational constants as the 0_0^0 band; hence, they must originate in the ZPL of the S_0 state. Thus, a HT mechanism involving the S_2 state must be responsible for the appearance of these vibronic bands. This is not a surprising result. That vibronic coupling involving nontotally symmetric modes is involved in the electronic spectra of NAPH and its derivatives has been known since the pioneering work of McClure.[2] (See also refs 4 and 8.) Presumably, the band at +422 cm^{-1} in ACN is the analog of the asymmetric in-plane distortion mode ($\overline{8}_0^1$) that appears at +433 cm^{-1} in the spectrum of NAPH (b_{1g} in Pariser's notation).[30] Its inertial defect in the S_1 state is −6.25 u Å^2, smaller in magnitude than the ZPL of the S_1 state, as is required for an in-plane mode. This mode transforms as a b_2 mode, according to the appropriate C_{2v} correlation table. The identity of the remaining modes is less clear. Figure 8 shows some possibilities. Ab initio frequency calculations (MP2 for the S_0 state and CIS for the S_1 state, with 6-31G** basis sets)[21] show that the +431 cm^{-1} band could be assigned to a (b_1 in C_{2v}) asymmetric out-of-plane CH rocking mode (theoretically expected at 450.2 cm^{-1}); it also has a negative inertial defect of −7.04 u Å^2, a more negative value than that of the 0_0^0 band. The +434 cm^{-1} band is likely to be a hot vibronic band; its ground state rotational constants are slightly different from those measured for the ZPL, and its rotational temperature is high (17 K), compared to the those measured for the other two bands (8−9 K). One possible

dx.doi.org/10.1021/jp1124298 |*J. Phys. Chem. A* 2011, 115, 9557–9566

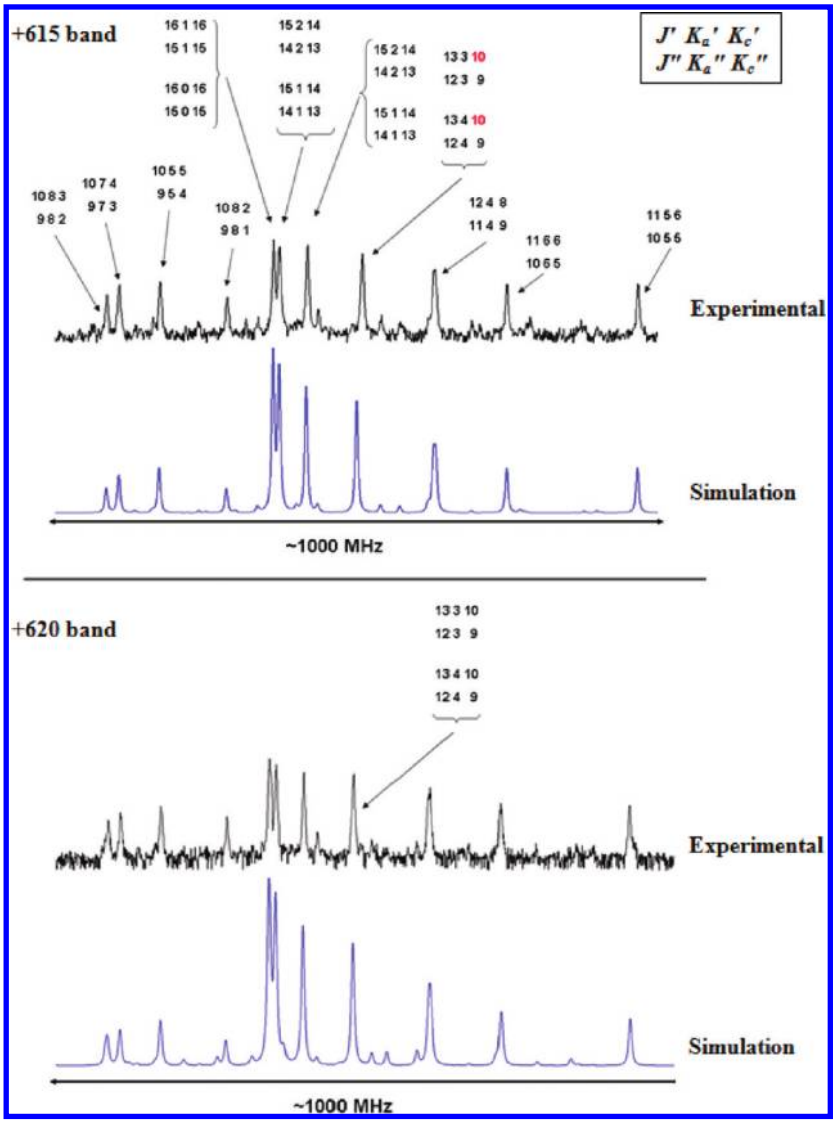

Figure 9. Similar portions of the *R* branch in the high resolution electronic spectra of the +615 and 620 bands of ACN. The simulated spectra show that the experimental traces exhibit anomalous intensity patterns on several rotational transitions. Some of the lines have been identified using their angular momentum quantum numbers, as indicated in the box.

assignment of this band is a combination of two nontotally symmetric vibrational modes; one of which should be the a_2 asymmetric CH_2-CH_2 bridge twisting mode (expected at 98.8 cm^{-1}) in the S_0 state and the b_1 asymmetric out-of-plane ring deformation mode (expected at 482.8 cm^{-1}) in the S_1 state. The inertial defects observed for this transition exhibits the largest negative value (−7.18 u $Å^2$) of all the bands studied in the S_1 state.

The vibronic bands appearing at +615 and 620 cm^{-1} above the 0_0^0 band of ACN exhibit *a*-type spectra (that is, their TDM orientations are the same as for the origin band). Neither band appears in the corresponding low-resolution spectrum of NAPH.[2,3] Portions of the *R* branches in the high resolution spectra of these two bands are shown in Figure 9. Some intensity anomalies have been observed in both spectra. For example, in the +615 cm^{-1} band, the doubly degenerate transitions with $J' \geq 7$ and K_a' or K_c' values less than 3 are weaker than expected [e.g., the transitions 16 0 16 (16 1 16) and 15 2 14 (15 1 14) in Figure 9], whereas the corresponding transitions with $J' \geq 7$ and K_a' greater than 4 are stronger than expected. The rovibronic lines with $K_a' = 3$ or 4 exhibit normal intensity patterns. Additionally, the transitions with $J' > 11$ and $K_c' = 10$ are special in terms of frequency; these lines were found to be shifted from their calculated positions, with increasing displacements as J' increases. An example of this effect is the line with quantum numbers 13 3 10 (13 4 10) in the top panel of Figure 9, where a small shift in frequency is detected. Lines with K_c =10 and $J' \leq 10$ do not exhibit any apparent frequency shifts. Similar anomalies in intensity (but not in frequency) were observed in the +620 cm^{-1} band. Rovibronic transitions with $J' > 10$ and $K_a' \leq 4$ or $J' > 14$ and $K_c \leq 3$ are weaker than expected (see bottom panel of Figure 9). In contrast, transitions with either $K_a' = K_c'$, $K_a' = K_c' \pm 1$ or $K_a' = K_c' \pm 2$ seem to be stronger than expected.

One possible source of these intensity anomalies, together with their overall intensity enhancement, is a Fermi resonance interaction[31] involving these two vibronic bands. A reasonable assignment of these two bands would be to the a_1 totally symmetric in-plane breathing mode, expected at 605 cm^{-1} for the +615 band, and to a combination of the b_1 asymmetric

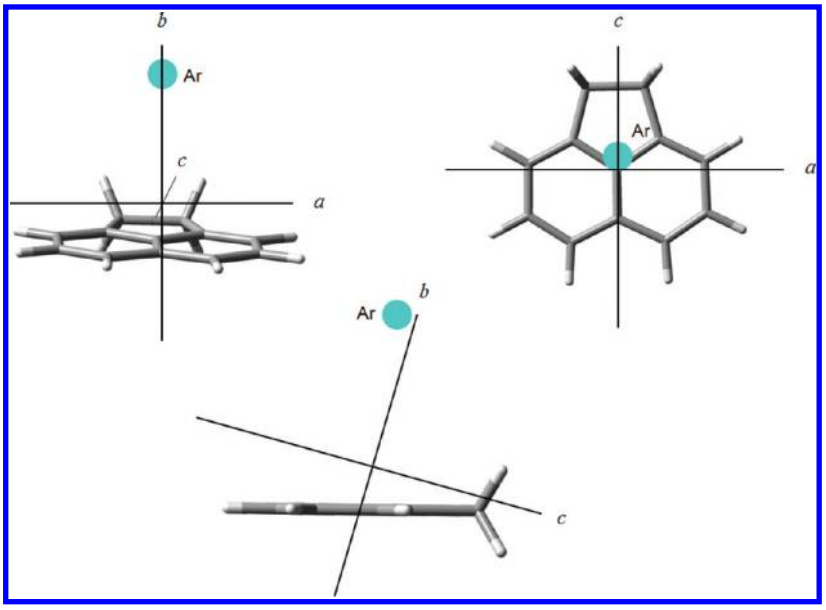

Figure 10. Relative position of the Ar atom in the ACN−Ar complex in its S_0 electronic state. The inertial axes are shown as a reference framework.

butterfly mode (expected at 159 cm^{-1}) and the b_1 asymmetric ring deformation mode (expected at 450 cm^{-1}) for the +620 band, see Figure 8. Their experimental zero-order frequency separation was found to be only ∼5 cm^{-1}, their polarizations within the C_{2v} point group are the same, and their inertial defects are −6.87 and −6.84 u $Å^2$, respectively. While the fundamental band might be strong, and the combination band weak, in zero order, a resonance interaction between the two modes could results in the two vibronic bands having nearly equal intensities, as observed (cf. Figure 1). A similar interaction plays a key role in the dynamical behavior of the analogous DHPH molecule in its S_1 state.[16]

Ar van der Waals Complex. Extensive investigations of noncovalent interactions have focused on weakly bound rare gas complexes of aromatic molecules.[32] Such complexes are of particular interest since the rare gas acts as a structureless probe of the shape of the intermolecular energy surface. Structural and dynamical studies of vdW molecular systems also provide information needed to elucidate the nature of weak chemical forces that dominate their behavior. In the present study, experimental information about the ACN−Ar vdW complex was obtained from a Kraitchman[33] analysis of the inertial parameters obtained from the fit of its rotationally resolved electronic spectrum in Figure 5 (see Table 2). This shows that the Ar atom is located 3.48 Å away from the center of mass of the ACN frame in its S_0 state (see Figure 10) and 3.44 Å away in its S_1 electronic state. These results are consistent with the rotation of the inertial axes that is observed on complex formation (cf. Figure 10), and with the fact that the TDM vector of the complex makes an angle of about 18° (2) with respect to its *c*-inertial axis.

Three additional studies seem relevant here. The first is the experimental work of Troxler and Leutwyler,[34] who found that naphthalene readily forms vdW complexes with Ar, and that the spectral red shifts of the origin and vibronic bands of the NAPH-Ar_n clusters are very small, −14 cm^{-1} with $n = 1$. The results for ACN−Ar are nearly the same; the binding energy of the attached Ar atom is only slightly larger in the S_1 state. Second, significantly larger red shifts have been observed in some systems; for example, 63 cm^{-1} in *trans*-stilbene−Ar.[35] And third is the theoretical study of Bacic and co-workers,[36] who found using DVR methods that the potential energy surfaces of complexes of this sort are very flat and exhibit multiple minima, making the isolation of localized bound states rather improbable. In ACN−Ar, we find that the in-plane Kraitchman coordinates of the Ar atom, when projected on the ACN plane, lie very close to the C_2 axis and are only slightly displaced toward the five-membered ring (see Figure 10). Extensive vibrational averaging is therefore implicated in the motion of the attached Ar atom with respect to the aromatic plane, evidence for which is the need to incorporate distortion terms in the fit of the rotationally resolved spectrum of ACN−Ar.

5. SUMMARY

Three different state mixing mechanisms have been observed in the first (S_1) electronically excited state of acenaphthene (ACN) by careful analyses of its rotationally resolved electronic spectra in the gas phase. These include an incomplete cancellation of the two one-electron excitations that contribute to the S_1 state, leading to an increased intensity of its electronic origin band, Herzberg−Teller coupling to the second (S_2) electronically excited state by nontotally symmetric vibrations, and a Fermi resonance involving different zero-order vibrational modes in the S_1 state. While the higher symmetry naphthalene molecule also exhibits HT coupling, the number of coupling routes is larger in the lower symmetry acenaphthene molecule. The $-CH_2-CH_2-$ "bridge" between the two rings also creates new low frequency modes that participate in the dynamics, not only in ACN itself, but also in the van der Waals complex ACN−Ar. It is likely that other processes will be exposed by further high resolution studies of this interesting molecule.

■ AUTHOR INFORMATION

Corresponding Author

*E-mail: leoav@fisica.ugto.mx.

■ ACKNOWLEDGMENT

This work has been supported by NSF (CHE-0615755 and CHE-0911117) to whom we are grateful. L. Alvarez-Valtierra appreciates the financial support provided by AMC/FUMEC 2010.

■ REFERENCES

(1) Dewar, M. J. S.; Longuet-Higgins, H. C. *Proc. Phys. Soc., London* **1954**, *67*, 795.
(2) McClure, D. S. *J. Chem. Phys.* **1954**, *22*, 1668. **1956**, *24*, 1.
(3) Beck, S. M.; Powers, D. E.; Hopkins, J. B.; Smalley, R. E. *J. Chem. Phys.* **1980**, *73*, 2019.
(4) Majewski, W. A.; Meerts, W. L. *J. Mol. Spectrosc.* **1984**, *104*, 271. See also Joo, D.-L.; Takahashi, R.; O'Reilly, J.; Kato, H.; Baba, M. *J. Mol. Spectrosc.* **2002**, *215*, 155.
(5) Johnson, J. R.; Jordan, K. D.; Plusquellic, D. F.; Pratt, D. W. *J. Chem. Phys.* **1990**, *93*, 2258.
(6) Berden, G.; Meerts, W. L.; Kreiner, W. *Chem. Phys.* **1993**, *174*, 247.
(7) Jagannathan, S.; Pratt, D. W. *J. Chem. Phys.* **1994**, *100*, 1874.
(8) Humphrey, S. J.; Pratt, D. W. *Chem. Phys. Lett.* **1996**, *257*, 169.
(9) Berden, G.; Meerts, W. L.; Plusquellic, D. F.; Fujita, I.; Pratt, D. W. *J. Chem. Phys.* **1996**, *104*, 3935.
(10) Semba, Y.; Yoshida, K.; Kasahara, S.; Ni, C.-H.; Hsu, Y.-C.; Lin, S. H.; Ohshima, Y.; Baba, M. *J. Chem. Phys.* **2009**, *131*, 024303.
(11) Baba, M.; Saitoh, M.; Taguma, K.; Shinohara, K.; Yoshida, K.; Semba, Y.; Kasahara, S.; Nakayama, N.; Goto, H.; Ishimoto, T.; Nagashima, U. *J. Chem. Phys.* **2009**, *130*, 134315.
(12) Craig, D. P.; Gordon, R. D. *Proc. R. Soc., London* **1965**, *288*, 69.
(13) van Herpen, W. M.; Meerts, W. L.; Dymanus, A. *J. Chem. Phys.* **1987**, *87*, 182.
(14) Baba, M.; Saitoh, M.; Kowaka, Y.; Taguma, K.; Yoshida, K.; Semba, Y.; Kasahara, S.; Yamanaka, T.; Ohshima, Y.; Hsu, Y.-C.; Lin, S. H. *J. Chem. Phys.* **2009**, *131*, 224318.
(15) Kowaka, Y.; Suganuma, Y.; Ashizawa, N.; Nakayama, N.; Goto, H.; Ishimoto, T.; Nagashima, U.; Baba, M. *J. Mol. Spectrosc.* **2010**, *260*, 72.
(16) Alvarez-Valtierra, L.; Pratt, D. W. *J. Chem. Phys.* **2007**, *126*, 224308.
(17) Majewski, W. A.; Pfanstiel, J. F.; Plusquellic, D. F.; Pratt, D. W. *Laser Techniques in Chemistry*; Rizzo, T. R., Myers, A. B., Eds.; J. Wiley & Sons: New York, 1995; p 101.
(18) Kato, H. et al. *Doppler-free high resolution spectral atlas of the iodine molecule*; Japan Society for the Promotion of Science: Tokyo, 2000.
(19) Chakraborty, T.; Chowdhury, M. *Chem. Phys.* **1992**, *159*, 439.
(20) Borisevich, N. A.; Vodovatov, L. B.; D'jachenko, G. G.; Petukhov, V. A.; Semenov, M. A. *Opt. Spektrosk.* **1996**, *81*, 757.
(21) Frisch, M. J. et al. *Gaussian 03*, Revision B.05; Gaussian, Inc.: Pittsburgh, PA, 2003.
(22) Plusquellic, D. F. *jb95 Spectral Fitting Program*; NIST: Gaithersburg, MD, http://physics.nist.gov/jb95 (accessed 2004-2010).
(23) Watson, J. K. G. *J. Chem. Phys.* **1968**, *48*, 4517.
(24) Salem, L. *The Molecular Orbital Theory of Conjugated Systems*; Benjamin: New York, 1966; p 397.
(25) Yi, J. T.; Alvarez-Valtierra, L.; Pratt, D. W. *J. Chem. Phys.* **2006**, *124*, 244302.
(26) Platt, J. R. *J. Chem. Phys.* **1949**, *17*, 484.
(27) Herzberg, G.; Teller, E. *Z. Phys. Chem.* **1933**, *21*, 410.
(28) Kuepper, J.; Pratt, D. W.; Meerts, W. L.; Brand, Ch.; Tatchen, J.; Schmitt, M. *Phys. Chem. Chem. Phys.* **2010**, *12*, 4980.
(29) Brand, Ch.; Oeltermann, O.; Pratt, D. W.; Weinkauf, R.; Meerts, W. L.; van der Zande, W.; Kleinermanns, K.; Schmitt, M. *J. Chem. Phys.* **2010**, *133*, 024303.
(30) For a comparison between Pariser's and Mulliken's notations on coordinate labeling in naphthalene molecule see Stockburger, M.; Gattermann, H.; Klusmann, W. *J. Chem. Phys.* **1975**, *63*, 4519.
(31) McHale, J. L. *Molecular Spectroscopy*; Prentice Hall: Upper Saddle River, NJ, 1999; p 296.
(32) For a recent review, see Kang, C.-H.; Pratt, D. W. *Intl. Rev. Phys. Chem.* **2005**, *24*, 1.
(33) Kraitchman, J. *Am. J. Phys.* **1953**, *21*, 17.
(34) Troxler, T.; Leutwyler, S. *J. Chem. Phys.* **1991**, *95*, 4010.
(35) Champagne, B. B.; Plusquellic, D. F.; Pfanstiel, J. F.; Pratt, D. W.; van Herpen, W. M.; Meerts, W. L. *Chem. Phys.* **1991**, *156*, 251.
(36) Mandziuk, M.; Bacic, Z. *J. Chem. Phys.* **1993**, *98*, 7165.